Biomedical Signal Processing and Control 31 (2017) 127–138

Contents lists available at ScienceDirect

Biomedical Signal Processing and Control

journal homepage: www.elsevier.com/locate/bspc

Characterization of cochlear implant artifacts in electrically evoked auditory steady-state responses

Hanne Deprez[a,b,*], Robin Gransier[a], Michael Hofmann[a], Astrid van Wieringen[a], Jan Wouters[a], Marc Moonen[b]

[a] KU Leuven, Experimental ORL, Dept. Neurosciences, Herestraat 49, 3000 Leuven, Belgium
[b] KU Leuven, STADIUS, Dept. Electrical Engineering (ESAT), Kasteelpark Arenberg 10, 3000 Leuven, Belgium

ARTICLE INFO

Article history:
Received 18 March 2016
Received in revised form 23 June 2016
Accepted 26 July 2016
Available online 1 August 2016

Keywords:
Cochlear implant (CI)
CI stimulation artifacts
Electrically evoked auditory steady-state responses (EASSR)
Linear interpolation
Monopolar mode stimulation

ABSTRACT

Objective: Electrically evoked auditory steady-state responses (EASSRs) are neural potentials measured in the electroencephalogram (EEG) in response to periodic pulse trains presented, for example, through a cochlear implant (CI). EASSRs could potentially be used for objective CI fitting. However, EEG signals are contaminated with electrical CI artifacts. In this paper, we characterized the CI artifacts for monopolar mode stimulation and evaluated at which pulse rate, linear interpolation over the signal part contaminated with CI artifact is successful.
Methods: CI artifacts were characterized by means of their amplitude growth functions and duration.
Results: CI artifact durations were between 0.7 and 1.7 ms, at contralateral recording electrodes. At ipsilateral recording electrodes, CI artifact durations are range from 0.7 to larger than 2 ms.
Conclusion: At contralateral recording electrodes, the artifact was shorter than the interpulse interval across subjects for 500 pps, which was not always the case for 900 pps.
Significance: CI artifact-free EASSRs are crucial for reliable CI fitting and neuroscience research. The CI artifact has been characterized and linear interpolation allows to remove it at contralateral recording electrodes for stimulation at 500 pps.

1. Introduction

A cochlear implant (CI) is an electronic device that can restore hearing in severely hearing impaired subjects. A CI system consists of three main parts: an external speech processor, the implant, and an electrode array inserted in the cochlea. The speech processor converts the incoming sound to an electrical stimulation pattern, which is transmitted to the implant via a radio frequency (RF) link. The electrodes stimulate the auditory nerve with biphasic charge-balanced pulses [1]. Two stimulation modes are often used, depending on the return electrode: bipolar mode for stimulation between intra-cochlear electrodes and monopolar mode for stimulation between intra- and extra-cochlear electrode(s). In clinical settings, pulses are often delivered at high rates in monopolar mode, which requires less battery power than stimulation in bipolar mode. Furthermore, threshold levels vary less over stimulation electrodes with stimulation in monopolar compared to bipolar mode, resulting in easier CI fitting.

Since early implantation is proven crucial for speech and language development (e.g. [2]), an increasing number of severely hearing impaired infants receive a CI within the first year of life. Prior to CI activation, the threshold (T) and maximum comfortable (C) stimulation levels are determined based on behavioral (verbal) feedback. This is particularly challenging in infants and subjects who cannot give reliable behavioral feedback. In such cases, objective CI fitting based on electrophysiological measurements could be used.

Objective CI fitting based on electrophysiological measurements is currently under investigation. Transient responses to low-rate stimuli measured at the electrode-nerve interface (ECAPs) and at the brainstem level (EABRs) have been investigated as objective measures for threshold estimation. However, the

Abbreviations: AGF, amplitude growth function; C, maximum comfortable stimulation level; CI, cochlear implant; d, interpolation duration; D, STIM artifact duration; EABR, electrically evoked auditory brainstem response; (E)ASSRs, (electrically evoked) auditory steady-state responses; ECAP, electrically evoked compound action potential; I, intercept of the CI artifact AGF; ICA, independent component analysis; PCA, principal component analysis; POD, programming device; RF, radio frequency; RF artifact, RF communication link artifact; STIM artifact, electrical stimulation artifact; T, threshold stimulation level; θ, slope of the CI artifact AGF.

* Corresponding author at: KU Leuven, STADIUS, Dept. of Electrical Engineering (ESAT), Kasteelpark Arenberg 10 bus 2446, 3001 Leuven, Belgium.
E-mail address: hanne.deprez@esat.kuleuven.be (H. Deprez).

http://dx.doi.org/10.1016/j.bspc.2016.07.013

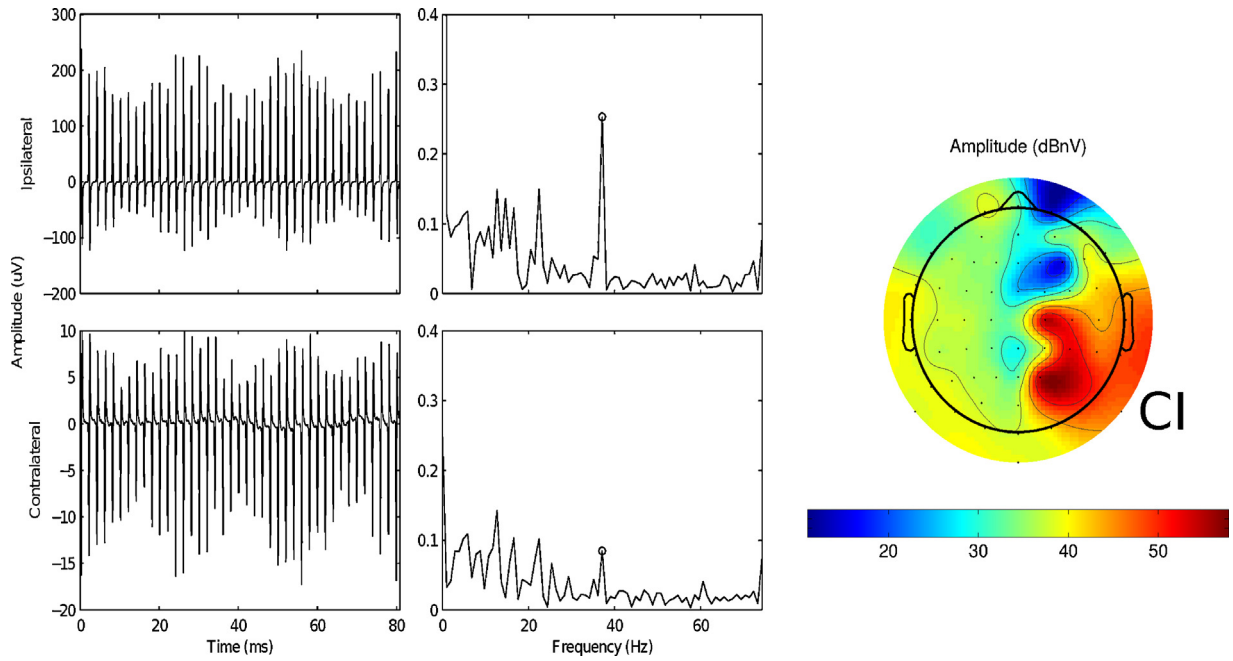

Fig. 1. Example of a CI artifact for S8, with a CI at the right side, measured with 37 Hz AM 900 pps pulse trains at a subthreshold stimulation amplitude. Left: time and frequency domain signals at recording electrodes TP_8 (ipsilateral) and TP_7 (contralateral), referenced to C_z. Right: spatial distribution of spectral power at the modulation frequency, referenced to C_z. The units of the topography plot are dBnV = 20 $\log_{10}$ nV, where 1 μV corresponds to 60 dBnV and 0.1 μV corresponds to 40 dBnV. No neural response is expected to be present, as subthreshold stimulation levels were used.

threshold values obtained with these methods that use low-rate stimuli are only moderately correlated with behavioral thresholds to high-rate pulse trains [3–6].

Objective CI fitting based on electrically evoked auditory steady-state responses (EASSRs) is also being researched. EASSRs are neural steady-state responses to electrical stimuli with a periodicity, such as a modulated pulse train. They are the electrical analogue of auditory steady-state responses (ASSRs), which are evoked acoustically, and can be recorded with head mounted scalp electrodes. ASSRs are the result of neural phase-locking to an auditory stimulus and the response is believed to result from different brain regions, depending on the repetition or modulation frequency of the stimulus (further called response frequency) [7,8]. (E)ASSRs can be detected in the frequency domain at the response frequency by means of a statistical test, e.g. an F-test or a Hotelling T^2 test [9,8].

EASSRs are corrupted by electrical stimulation artifacts, which can be caused by both the electrical stimulation pulses and the RF communication link between the external speech processor and the implant. The former can have a periodic component at the response frequency which may distort the neural response [12]. Fig. 1 shows the EEG signal recorded on two channels in time and frequency domain, for subthreshold stimulation. Both EEG signals have a component at the modulation frequency, which is caused by the electrical stimulation since no neural response is believed to be present. The spatial distribution of the spectral component at the modulation frequency is shown in the topography plot, indicating that the electrical stimulation artifact is present on all recording electrodes. The amount of distortion is highly subject-dependent, and is affected by the stimulation parameters and the recording electrode positions. Stimulation in monopolar mode results in larger CI artifacts than in bipolar mode [10,11].

It was recently demonstrated that EASSRs in response to high-rate stimuli result in electrophysiological thresholds that correlate well with behavioral thresholds for stimulation in bipolar mode [12]. The next step is to evaluate threshold estimation based on EASSRs for clinically used parameters, in particular for stimulation in monopolar mode.

Stimulation artifacts contaminating the EEG are a problem in various domains where electrical or magnetic stimulation is used, including deep brain stimulation, transcranial magnetic and current stimulation, somatosensory and cochlear implant stimulation.

Changes to the measurement set-up, such as maximum separation of stimulation and recording electrode leads, proper grounding of amplifier and subject, and careful skin preparation can help to reduce artifact amplitudes [10,13]. However, none of these measures can completely prevent the presence of excessive stimulation artifacts in the EEG. Optimal reference electrode placement has been investigated for transient responses to cochlear implant stimulation [14], but optimal selection of reference electrode has not yet been assessed for artifact removal in EASSR measurements. Stimulus design can also help to avoid stimulation artifacts: responses to alternating polarity pulses have been averaged in order to reduce the stimulation artifact [15,16], or short stimuli have been used such that the stimulation artifact has decayed before the response occurs [16]. Adjustments to the stimuli are not desirable in our case, because we aim to measure EASSRs to clinically used stimuli. Therefore, stimulation is restricted to cathodic-first, biphasic pulses, with fixed pulse width and interphase gap, presented at high rates and in monopolar mode.

Artifact elimination methods remove EEG channels or epochs that are contaminated with artifact. This is done for example with ocular artifacts in the EEG. However, all epochs are affected by stimulation artifacts in EASSR measurements because of the continuous stimulation. Furthermore, most recording channels are affected by stimulation artifact. Therefore, artifact elimination methods are not appropriate for artifact removal in EASSR measurements, since almost all data would be rejected.

Several methods have been proposed for stimulation artifact minimization. Single channel techniques include frequency [17], time–frequency [18–20], or adaptive filtering [21–26]. Template subtraction [27–30] has also been investigated. In the case of EASSR, frequency domain filtering is inappropriate because the stimulation artifact has a component at the response frequency. For adaptive filtering and template subtraction, assumptions

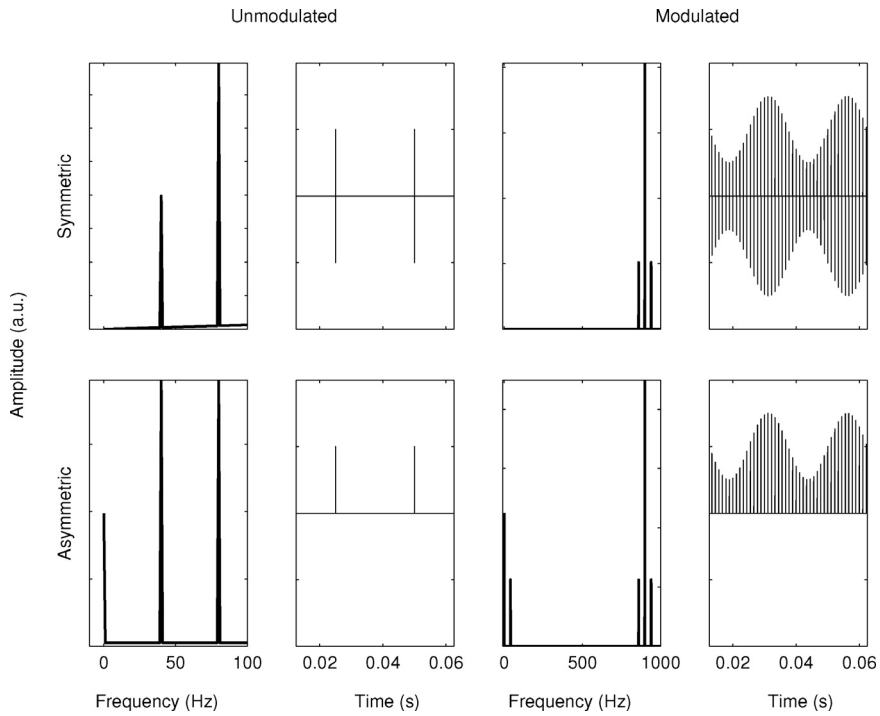

Fig. 2. Simulated CI artifact spectrum for unmodulated pulse trains presented at a repetition frequency of 40 pps (left) and for high-rate (900 pps) 40 Hz AM pulse trains (right), in the case of symmetric (top) and asymmetric CI artifacts (bottom).

concerning the stimulation artifact shape or filtering process need to be made.

Interpolation methods [31,32,10,12] have also been used. For time-restricted stimulation artifacts, an interpolation can be applied between a pre-artifact and post-artifact sample, effectively removing the stimulation artifact. This method is only successful if the interpulse interval is larger than the stimulation artifact duration, and it has been validated for EASSR measurements in bipolar stimulation mode.

Multichannel techniques such as beamforming [33], principal (PCA) [16] and independent component analysis (ICA) [14,16,34–41] were investigated in various domains. CI stimulation artifacts have successfully been removed from the EEG for transient responses using multichannel methods, but these methods have not yet been investigated for steady-state responses. Clinically, multichannel EEG systems are expensive and require more subject preparation time.

The aim of this study is to characterize the CI artifact for modulated high-rate pulse trains stimulated in monopolar mode and investigate the feasibility of stimulation artifact removal with linear interpolation. Modulated pulse trains are a model for the electrical pulse sequences after processing of speech by the CI processor. Linear interpolation was chosen as the CI artifact removal method, because its efficiency has been demonstrated for bipolar stimulation, and it can be applied to single channel data. The CI artifact characterization will help to explore the feasibility of other above mentioned CI artifact removal methods. The influence of reference electrode position on the CI artifact characteristics and the operating limits of the interpolation method will be investigated.

2. Materials and methods

The CI artifact consists of two main parts from the RF communication link (the RF artifact) and from the electrical stimulation (the STIM artifact). The CI artifact is time-locked to the electrical stimulation pulse and can contain a frequency component at the modulation frequency [10,12], as can be seen in Fig. 1 for recorded data and Fig. 2 for simulated cases. This may result in distorted EASSR properties such as amplitude and phase and false positive EASSR detections.

In Cochlear Nucleus® implants, the stimulation amplitude of the pulses is nonlinearly encoded in the RF transmission and is therefore constant for stimulation pulses with different amplitudes [28], whereas the STIM artifact amplitude is related to the stimulation pulse amplitude. For stimulation with unmodulated pulse trains, both the RF and the STIM artifact are present at the response frequency (namely the repetition frequency of the stimulation pulses). For stimulation with high-rate modulated pulse trains, only the STIM artifact is present at the response frequency (namely the modulation frequency of the stimulation pulses). Furthermore if the STIM artifact is symmetric, no STIM artifact will be present at the response frequency, as can be seen in Fig. 2. In the following, we only consider stimulation with high-rate modulated pulse trains. In this case, only the STIM artifact components are problematic for EASSR measurements as they may have a contribution at the modulation frequency.

The scaling of the CI artifacts with increasing stimulation amplitude is quantified by means of the slope of the CI artifact amplitude growth function (AGF). If the slope is zero, the CI artifacts do not scale with changing stimulation amplitude, which indicates that they will not be present at the modulation frequency. If CI artifacts are present at the modulation frequency, they can possibly be removed with a linear interpolation. However, this only works if the CI artifact is shorter than the interpulse interval. Therefore, the STIM artifact duration is also quantified.

EASSRs were measured in 11 subjects with a Cochlear Nucleus® CI with stimulation below the subject's behavioral threshold level. Details about subjects, stimulation, and recording setup are described in Sections 2.1, 2.2 and 2.3, respectively. CI artifact AGF intercepts and slopes and STIM artifact durations were determined

Table 1
List of subjects with Cochlear Nucleus® implant details. S: subject identifier; Sex: M: male, F: female; Age: age in years; Exp: CI experience in years; Side of implantation: R: right, L: left; PR: pulse rate tested.

S	Sex	Age	Exp	Implant type	Side	PR	
						500 pps	900 pps
S1	F	55	16	CI24R	L		x
S2	M	64	11	CI24R	L	x	x
S3	M	19	17	CI24M	L		x
S4	F	85	5.7	CI24R	L	x	x
S5	M	74	1.2	CI24RE	R		x
S6	M	52	1.7	CI24RE	R	x	
S7	M	64	16	CI24R	L	x	x
S8	M	52	1.9	CI24RE	R	x	x
S9	F	44	0.5	CI422	R	x	x
S10	F	77	1.9	CI24Re	L	x	
S11	F	63	2.5	CI24RE	R	x	

for all subjects as described in Section 2.4. All signal processing and statistical analyses were done in *MATLAB R2013a*.

2.1. Subjects

In total, 11 adult subjects participated in the experiments. They all had a Cochlear Nucleus® CI. Details can be found in Table 1. All subjects took part voluntarily and signed an informed consent form. The experiments were approved by the medical ethics committee of the University Hospitals Leuven (approval number B32220072126).

2.2. Stimulation setup

An in-house developed stimulation software platform generated the electrical stimulation pulse sequences with specified stimulation parameters, such as pulse rate, modulation frequency, stimulation electrode, etc. [10]. The electrical pulse sequences were sent to a programming device (POD) connected to a L34 research speech processor provided by Cochlear Ltd., thereby bypassing the subject's clinical speech processor.

Cochlear Nucleus® implants have two return electrodes outside the cochlea, i.e. the casing and the ball electrode. All subjects were stimulated in monopolar mode MP1+2, i.e. between an intracochlear electrode and the two extracochlear return electrodes which are electrically coupled [42]. An intracochlear electrode in the middle of the array was used: electrode 11 was used for all subjects except S1, for whom electrode 13 was used. The stimuli consisted of amplitude-modulated (AM) pulse trains with modulation frequencies in the 40 Hz-range, which is often used for testing adults because large responses are expected here. Clinically used symmetric biphasic pulses with a pulse width of 25 μs and an interphase gap of 8 μs were used for stimulation.

Threshold and comfort levels were determined for stimulation with unmodulated (T_u and C_u) and AM pulse trains (T_m and C_m). The T level is the stimulation amplitude (in Cochlear clinical current units (cu), a unit of electrical current) that elicits a just perceivable auditory perception. The C level is the stimulation amplitude at perceived maximum comfortable loudness. For AM pulse trains, the determined T_m and C_m refer to the maximum amplitude of the AM pulse trains that result in a just perceivable auditory sensation and a maximally comfortable sound, respectively.

Two stimulation pulse rates were tested: 500 pps which is at the lower end of clinically used stimulation, and 900 pps which is the default pulse rate used in Cochlear Nucleus® implants. The stimuli were modulated with frequencies in the 40 Hz range. Subjects were stimulated at subthreshold stimulation pulse train intensities, with modulation depth equal to $(C_m - T_u)/(C_m + T_u)$, during 5 min.

2.3. Recording setup

To study the effect of reference electrode position, a 64-channel active-electrode BioSemi ActiveTwo DC EEG recording system was used. The system has a 24 bit resolution over a dynamic range of 524 mV_{PP} and a sampling rate of 8192 Hz was used. The recording setup has a built-in analog 5th order sinc low-pass filter with a cutoff frequency of 1638 Hz. Recording electrodes were placed on the subject's head according to the positions of the international 10–20 system [43]. A trigger signal was sent to the recording system for synchronization at the beginning of each recording epoch of 1.024 *s*. After EEG signal recording during 5 min, the signals were rereferenced offline to three commonly used reference schemes: average reference, vertex reference C_z, and forehead reference Fp_z.

The recordings were made in a soundproof and electrically shielded room. Subjects were seated in a comfortable chair and were asked to move as little as possible. A silent but subtitled movie of their choice was played, to guarantee the same attentional state across subjects and measurements.

2.4. CI artifact characterization

2.4.1. CI artifact amplitude growth

The CI artifact AGF $A(A_s)$ shows how the CI artifact amplitude A changes with increasing stimulation pulse amplitude A_s.

The CI artifact amplitude A_p was determined for every stimulation pulse. Let $x_p(t, c)$ be the EEG signal following pulse p (with stimulation amplitude $A_s(p)$ μA) at time t and channel c. In the following, we will make abstraction of the channel c as the method can be applied to every channel separately. A_p (in μV) was defined as the sum of the pulse's maximal and minimal amplitude.

$$A_p = \left| \max_t \; x_p(t) + \min_t \; x_p(t) \right| \tag{1}$$

For symmetrical artifacts, with equal negative and positive amplitudes, A_p will be zero. For asymmetrical artifacts, A_p will differ from zero.

For each stimulation pulse p stimulated at amplitude $A_s(p)$, the maximal and minimal EEG amplitudes were determined and summed, resulting in A_p. Next, these values were averaged for all pulses presented at the same stimulation amplitude, such that one CI artifact amplitude A is determined for each stimulation pulse amplitude A_s. In a first approximation, the CI artifact AGF $A(A_s)$ can be modeled as a linear function of A_s: $A(A_s) = mA_s + I$ with intercept I and slope $m = \theta^\circ$, as shown in Fig. 3. The best linear fit was determined for every channel with a least squares procedure, resulting in values for the intercept I and slope θ.

The intercept I represents asymmetric CI artifact components that are constant across stimulation pulse intensities; these artifact components are mainly caused by the RF artifact. The slope θ represents asymmetric CI artifact components that change with increasing stimulation pulse amplitude, namely the STIM artifact. If the CI artifact is symmetric, both θ and I will be zero. If θ is zero and I is non-zero, the CI artifact is mainly caused by RF transmission. If both θ and I are non-zero, the CI artifact consists of RF and STIM artifact. Only the STIM artifact components are problematic for EASSR measurements as these are the only components that have a contribution at the modulation frequency.

A slope of 1° corresponds to an increase of 0.017 μV/μA. In this study, the stimulation amplitude range averaged over subjects is about 100 μA. Therefore, the amplitude difference between the largest and smallest pulse amplitude for $\theta = 1^\circ$ is 1.7 μV for an average subject. This is a large value, compared to the neural response which has amplitudes between 20 and 500 *nV* for average subjects in the 40 Hz range [12].

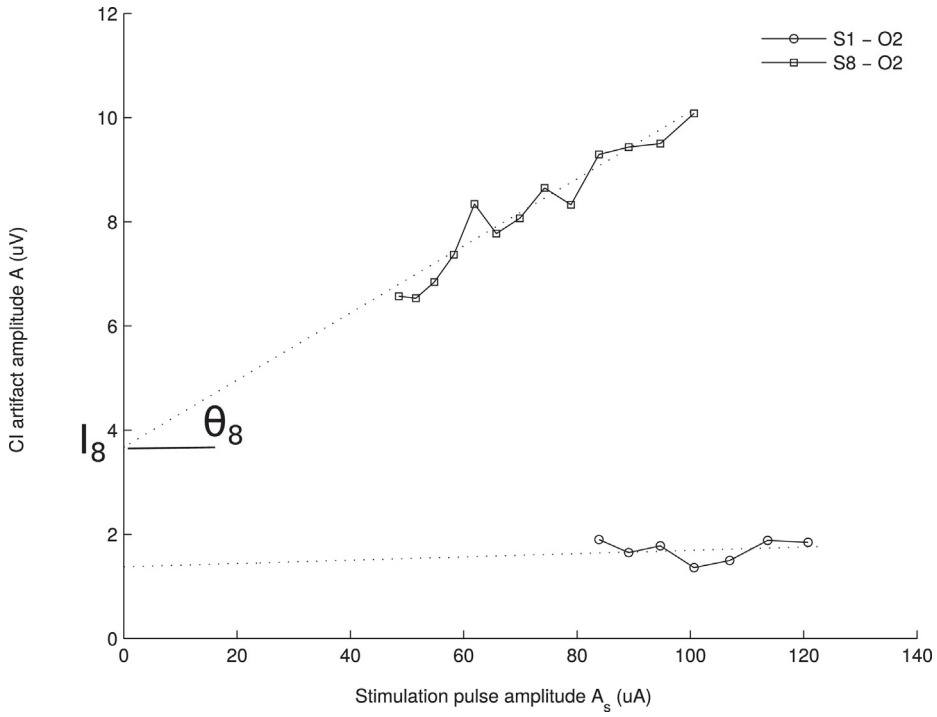

Fig. 3. CI artifact AGFs for S1 and S8, measured with 37 Hz AM 900 pps pulse trains at a subthreshold stimulation amplitude, between an ipsilateral occipital electrode (O_2) and forehead reference electrode (Fp_z).

CI artifact AGFs were constructed for all subjects. Examples of such AGFs are shown in Fig. 3. Pulse rates of 500 and 900 pps were used, although not all subjects were tested with stimulation at both pulse rates, as shown in Table 1. The DC bias was removed from the recorded EEG signals with a second-order 2 Hz high-pass filter and the EEG signals were rereferenced to either average reference, C_z, or Fp_z. The values of the intercept I and slope θ of the CI artifact AGF were determined for every recording channel and for different recording electrode configurations.

2.4.2. STIM artifact duration

Artifacts were removed by linear interpolation between a pre-stimulus and post-stimulus sample. The time between the pre- and post-stimulus sample is called the interpolation duration d. The maximum possible interpolation duration is defined as the inter-pulse interval, which is the inverse of the pulse rate, and equals 2 ms and 1.1 ms for stimulation at 500 and 900 pps, respectively. In this case, one sample per pulse period, the pre-stimulus sample, is retained. A linear interpolation was applied between the pre-stimulus sample at −100 μs and post-stimulus samples varying between +500 and +1900 μs, in steps of 100 μs for 500 pps. For 900 pps, post-stimulus samples varying between +500 and +900 μs, were used, in steps of 100 μs. The sampling rate is not an exact multiple of the pulse rate. Therefore, the start of a stimulation pulse is not exactly aligned to a sample. The start and end samples of the interpolation are calculated for each pulse separately, by rounding the start and end time of the interpolation to the nearest sample. Looking over the whole recording, the average time between the start of the interpolation interval and the start of a stimulation pulse is equal to the pre-stimulus interpolation duration. Equivalently, the average time between the start of a stimulation pulse and the end of the interpolation interval is equal to the post-stimulus interpolation duration. Post-stimulus samples before +500 μs were not used, as the CI artifact peak lasts for about 500 μs, as can be seen in Fig. 4.

After linear interpolation, the signals were filtered with a second-order 2 Hz high-pass filter, rereferenced to either average reference, C_z or Fp_z, and split into 1.024 s epochs. The 300 resulting epochs, corresponding to a 5 min recording length, were then averaged to reduce the noise level n. Then, the resulting spectral amplitudes A_m at the modulation frequency in function of the interpolation duration d were determined, as illustrated in Fig. 4.

When the interpolation duration is shorter than the STIM artifact, $A_m(d)$ may still contain some STIM artifact. However, $A_m(d)$ decreases with increasing interpolation duration, as a larger part of the STIM artifact is then canceled. When the interpolation duration is longer than the STIM artifact duration, $A_m(d)$ stabilizes at the neural response amplitude, namely the real EASSR amplitude. $A_m(d)$ stabilizes to the noise level, in our case, as no neural response is expected to be present for subthreshold stimulation.

An $A_m(d)$ AGF example is shown in Fig. 4. The differences in A_m for increasing interpolation duration d were compared to the noise level after averaging n. The STIM artifact duration D was defined as the shortest interpolation duration for which this difference did not exceed the subject dependent noise level n, which is approximately 50 nV:

$$D = d : [A_m(d) - A_m(d-1)] < n \quad (2)$$

If $A_m(d)$ did not saturate, meaning that the difference in $A_m(d)$ was not smaller than the noise level for any interpolation duration d, the STIM artifact duration D was set equal to the maximal interpolation duration.

2.4.3. Statistical analyses

The intercept I and slope θ of the CI artifact AGF and the STIM artifact duration D were determined as described above for all recording electrodes and for three reference electrode configurations in all subjects. Left and right recording electrodes were switched for subjects with a CI at the right hand side, to put the results in the same figure for subjects with a CI at the left and right

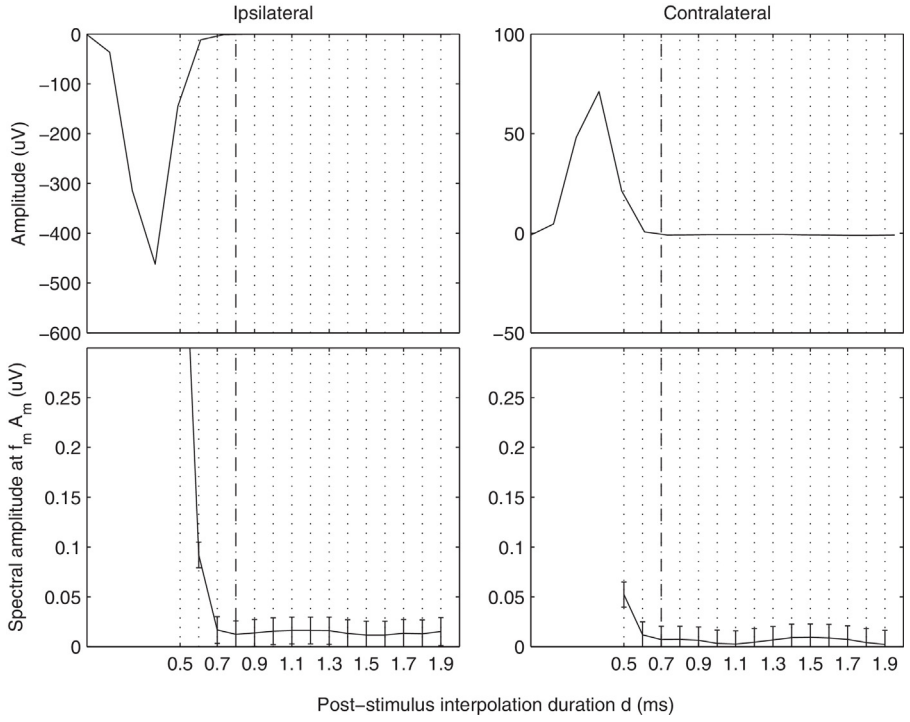

Fig. 4. CI artifact pulse (top) and $A_m(d)$ AGF with increasing interpolation duration d for subject S2 (bottom). Stimulation below T level at 500 pps, for ipsi- and contralateral recording electrodes. The STIM artifact durations are indicated in dash-dotted lines. Reference electrode C_z.

hand side. The resulting signals were averaged across all subjects to obtain the average CI artifact profile shown in Fig. 5. This may give a blurred view, as CI artifacts may be localized slightly differently in all subjects.

In the following, only recording electrodes located in the posterior part of the head (T_x, $C(P)_x$, $P(O)_x$, O_x, I_x) were considered. For each subject, the median value of θ, I and D over the recording electrodes was determined. A statistical analysis investigating the effect of reference electrode, hemisphere, and pulse rate on θ, I and D was carried out. All effects are reported at a significance level of 5%. The data were not normally distributed according to a Jarque–Bera test, and therefore only nonparametric tests were used. A Friedman analysis was used to investigate the effect of reference electrode on the CI artifact AGF slope and STIM artifact duration for each pulse rate and for each hemisphere. The effect of hemisphere was investigated using Wilkinson signed rank tests (averaging the results for reference electrodes C_z and Fp_z). The influence of pulse rate on CI artifact AGF slope and STIM artifact duration was checked for each

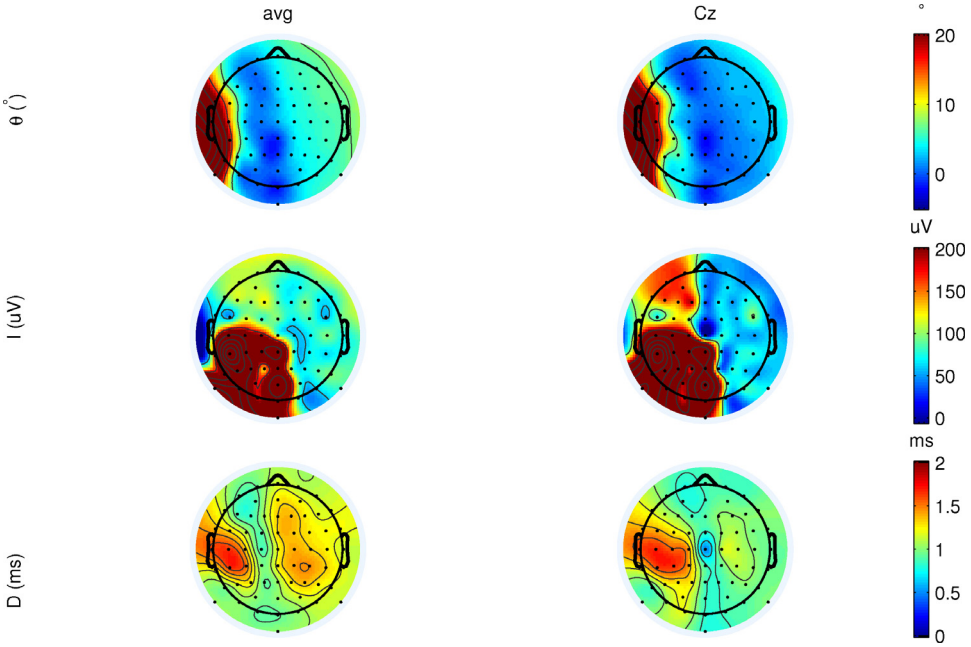

Fig. 5. Mean slope θ and intercept I of the CI artifact AGF and mean STIM artifact duration, averaged over all subjects with recordings with stimulation at 500 pps. Average reference (left column) and reference electrode C_z (right column).

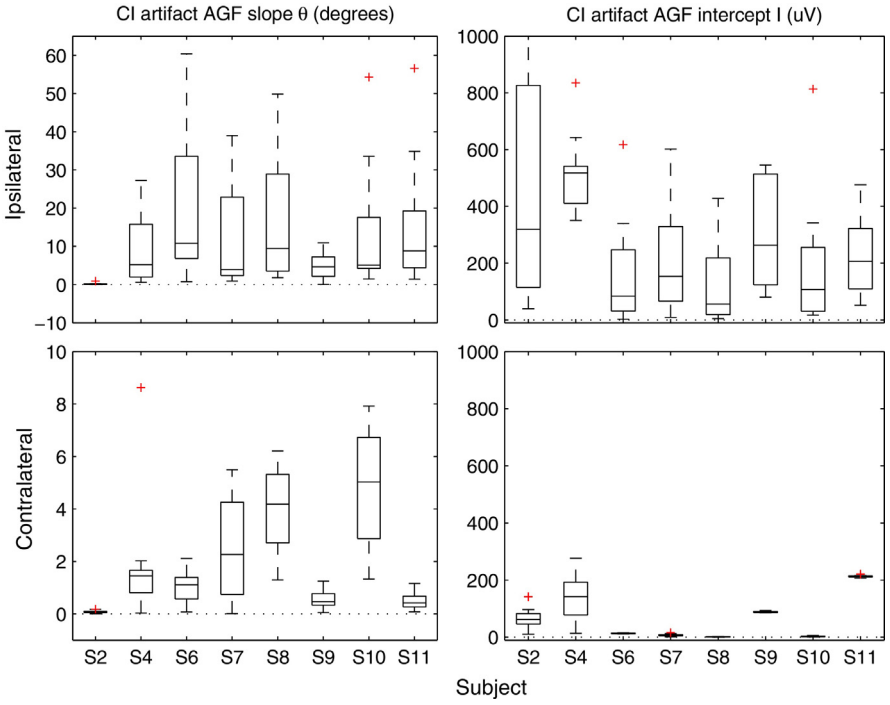

Fig. 6. CI artifact AGF slope θ and intercept I for ipsi- and contralateral posterior recording electrodes for each subject with recordings with stimulation at 500 pps. Reference electrode C_z. The boxplot shows the median and 25th (q_1) and 75th percentiles (q_3). Outliers (+) are all data points that fall outside the range $[q_1 \pm 1.5(q_3 - q_1)]$.

hemisphere (averaging the results for reference electrodes C_z and Fp_z), using Wilkinson rank sum tests.

3. Results

3.1. CI artifact AGF slope and intercept

CI artifact AGF slopes and intercepts are shown in Figs. 6 and 7. The CI artifact is symmetric if both θ and I are zero and this is only the case for subject S1 (Fig. 7).

Most subjects had a CI artifact AGF similar to that of subject S8 in Fig. 3. The CI artifact slope is different from zero, which means that the STIM artifact contributes to the CI artifact.

3.2. STIM artifact duration

Fig. 8 shows STIM artifact durations D for each subject separately, on all ipsilateral and contralateral posterior recording electrodes respectively. For stimulation at 500 pps, the median STIM artifact duration at the ipsilateral posterior electrodes is 1.6 ms, although the STIM artifact duration is close to or longer than 2 ms at some electrodes in some subjects (Fig. 8). For stimulation at 900 pps, the determined STIM artifact duration is equal to 1.1 ms in almost all subjects at ipsilateral recording electrodes. D is thus larger than the maximum possible interpolation duration.

At contralateral recording electrodes, the median STIM artifact duration is 1 and 0.9 ms at 500 and 900 pps, respectively. For stimulation at 900 pps, D is close or equal to 1.1 ms in some subjects (Fig. 8).

3.3. Influence of reference electrode and hemisphere

The slope θ and intercept I of the CI artifact AGF and the STIM artifact duration D are largest in the proximity of the implant (Fig. 5). θ, I and D are larger in the contralateral hemisphere for average reference than for reference electrode C_z.

For stimulation at 500 pps, a significant influence of reference electrode on CI artifact AGF slopes was found in the ipsilateral ($\chi^2(2) = 7.8$, $p = 0.021$) and the contralateral hemisphere ($\chi^2(2) = 6.8$, $p = 0.034$), see Fig. 9. In the ipsilateral hemisphere, larger CI artifact AGF slopes were found for the Fp_z reference electrode montage. In the contralateral hemisphere, more variation in CI artifact AGF slope is observed when reference electrode C_z is used compared to when reference electrode Fp_z is chosen. For stimulation at 900 pps, a significant influence of reference electrode on CI artifact AGF slopes was found in the ipsilateral hemisphere ($\chi^2(2) = 9$, $p = 0.011$) and in the contralateral hemisphere ($\chi^2(2) = 7$, $p = 0.030$).

For stimulation at 500 pps, a significant influence of reference electrode on CI artifact AGF intercept was found in the contralateral ($\chi^2(2) = 7$, $p = 0.030$), but not in the ipsilateral hemisphere ($\chi^2(2) = 1.0$, $p = 0.607$), see Fig. 10. In the contralateral hemisphere, smaller CI artifact AGF intercepts were found for the Fp_z reference. For stimulation at 900 pps, no significant influence of reference electrode on CI artifact AGF intercepts was found in the ipsilateral hemisphere ($\chi^2(2) = 1.75$, $p = 0.417$) or in the contralateral hemisphere ($\chi^2(2) = 0.75$, $p = 0.687$).

For stimulation at 500 pps, the reference electrode was found to have a significant influence on STIM artifact duration on ipsilateral ($\chi^2(2) = 6.1$, $p = 0.048$) and contralateral electrodes ($\chi^2(2) = 14.6$, $p < 0.001$). In the contralateral hemisphere, shorter STIM artifact durations were found for the Fp_z reference. In the ipsilateral hemisphere, the STIM artifact duration is larger than the maximum possible interpolation duration for stimulation at 900 pps. Therefore the influence of reference electrode on the STIM artifact duration was only checked in the contralateral hemisphere. The reference electrode was found to have a significant influence on STIM artifact durations in the contralateral hemisphere ($\chi^2(2) = 13.0$, $p = 0.002$). Shorter STIM artifact durations were again found for the Fp_z reference.

For stimulation at 500 pps there was a significant effect of hemisphere on CI artifact AGF slope, offset and STIM artifact duration ($p = 0.008$, $p = 0.008$, and $p = 0.008$, respectively). Prior

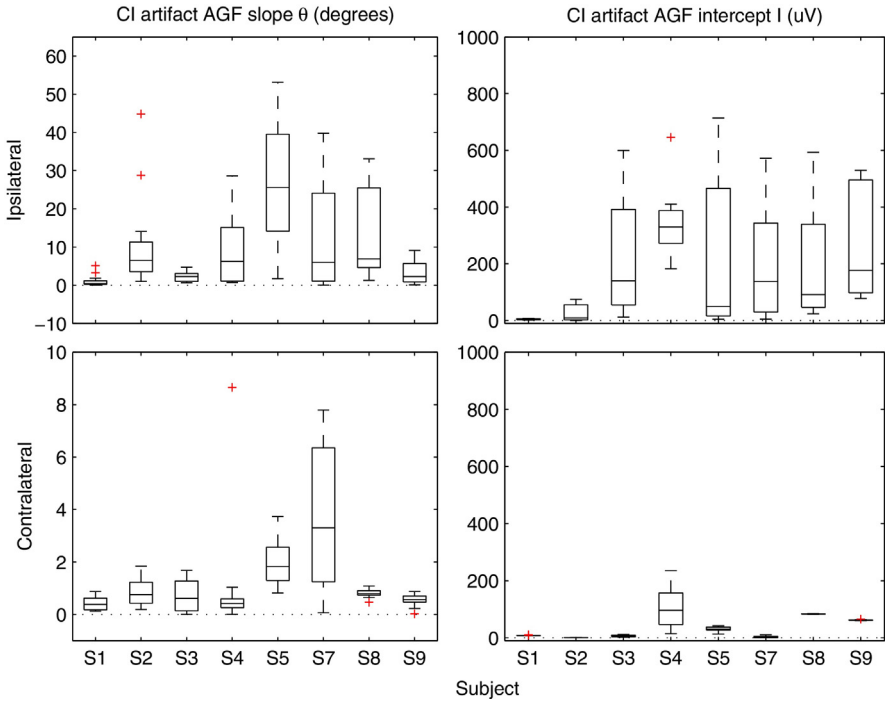

Fig. 7. CI artifact AGF slope θ and intercept I for ipsi- and contralateral posterior recording electrodes for each subject with recordings with stimulation at 900 pps. Reference electrode C_z.

to the statistical analysis results for reference electrodes C_z and Fp_z were averaged. For these reference electrodes, the CI artifact AGF slope is smaller and STIM artifact duration is shorter in the contralateral hemisphere. For stimulation at 900 pps, a significant effect of hemisphere was found on the CI artifact AGF slope and intercept ($p = 0.016$ and $p = 0.016$, respectively), with smaller CI artifact AGF slopes and intercepts in the contralateral hemisphere. The effect of hemisphere on STIM artifact duration could not be investigated, as the STIM artifact duration is longer than the maximal interpolation duration in the ipsilateral hemisphere.

3.4. Influence of pulse rate

No significant influence of pulse rate on CI artifact AGF slope was found, for neither of the hemispheres ($p = 0.798$ and $p = 0.721$ for ipsi- and contralateral hemisphere, respectively). No significant influence of pulse rate on CI artifact AGF intercept was found, for

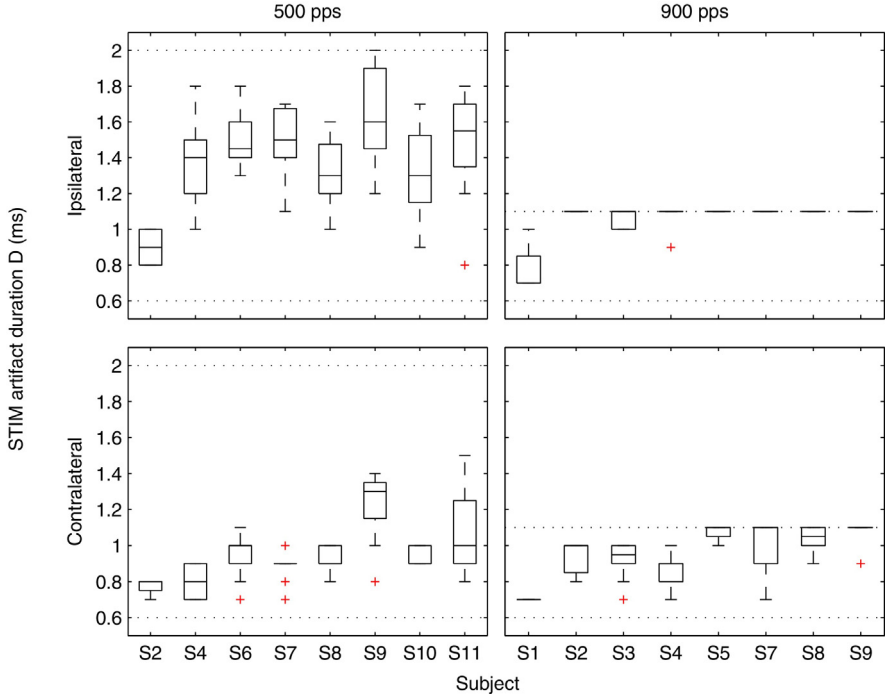

Fig. 8. STIM artifact duration for ipsi- and contralateral posterior recording electrodes for each subject with recordings with stimulation at 500 and 900 pps. Reference electrode C_z. Dotted lines indicate the minimum and maximum possible interpolation duration at 500 and 900 pps.

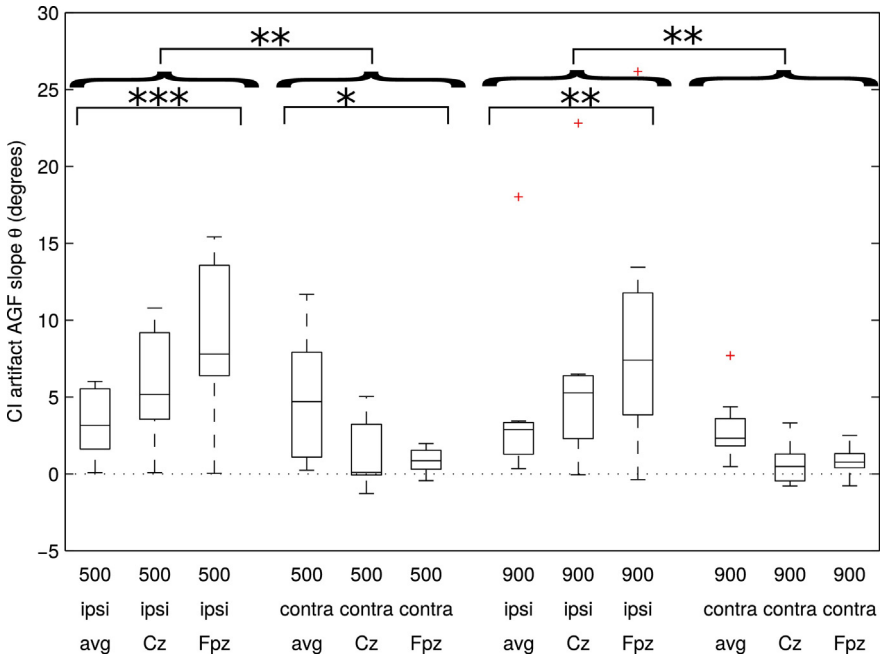

Fig. 9. CI artifact AGF slope θ per pulse rate (500 and 900 pps), hemisphere (ipsi- and contralateral) and reference electrode (average reference, C_z and Fp_z). The symbols *, **, and *** indicate that p-values are smaller than 0.05, 0.01, and 0.001, respectively.

neither of the hemispheres ($p = 0.235$ and $p = 0.328$ for ipsi- and contralateral hemisphere, respectively). No significant influence of pulse rate on STIM artifact duration was found in the contralateral hemisphere ($p = 0.343$). STIM artifact durations for both pulse rates could not be compared in the ipsilateral hemisphere, as the STIM artifact duration exceeded the maximum possible interpolation duration at 900 pps.

4. Discussion

In this study, the CI artifact was characterized based on three properties, namely, the CI artifact AGF slope and intercept and the STIM artifact duration. The CI artifact AGF slope and STIM artifact duration describe how the CI artifact scales with stimulation amplitude and how long it takes the STIM artifact to have decayed completely, respectively. Significantly larger CI artifact AGF slopes and intercepts and STIM artifact durations are found at ipsilateral recording electrodes than at contralateral ones. For electrodes positioned at the contralateral side, the reference electrode location can have an influence on the CI artifact AGF slope and intercept (for stimulation at 500 pps) and STIM artifact duration. No significant influence of pulse rate on any property has been found. Based on the STIM artifact durations (Fig. 8), it should be possible to remove STIM artifacts at contralateral electrodes with a linear interpolation for stimulation at 500 pps. For stimulation at 900 pps, more advanced methods are needed.

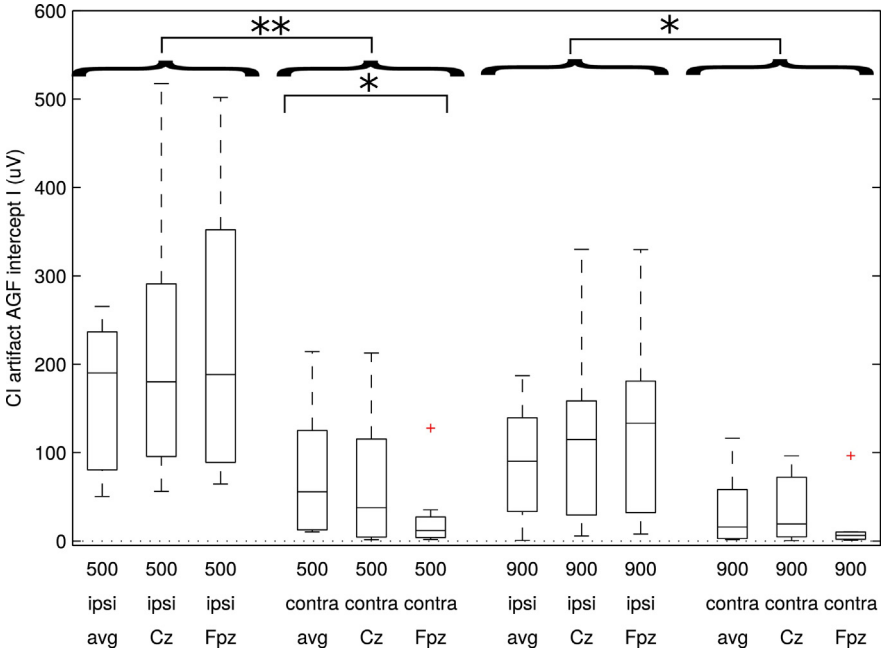

Fig. 10. CI artifact AGF intercept I per pulse rate (500 and 900 pps), hemisphere (ipsi- and contralateral) and reference electrode (average reference, C_z and Fp_z).

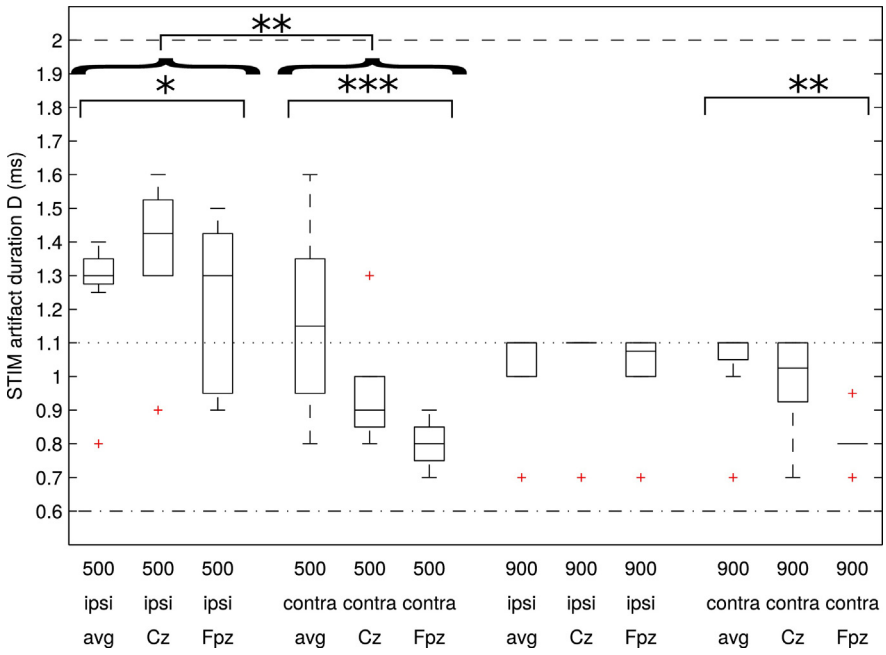

Fig. 11. STIM artifact duration per pulse rate (500 and 900 pps), hemisphere (ipsi- and contralateral) and reference electrode (average reference, C_z and Fp_z). Dashed and dotted lines indicate the maximum possible interpolation duration at 500 and 900 pps, respectively. The dash-dotted line indicates the minimum interpolation duration used for the analysis.

It is not recommended to use average reference subtraction with CI stimulation. When the subtracted reference contains more artifact than the channel from which it is subtracted, the resulting signal in that channel could contain more CI artifact after reference subtraction than before. Large CI artifact signals present at some electrodes will bias the mean signal over channels, resulting in large CI artifacts at all channels after reference subtraction.

The reference electrode has not only an influence on the CI artifact characteristics, but also on the detected EASSR. The source of the EASSRs is oriented along a dipole. In order to record reliable EASSRs with maximal amplitudes, the analysis and reference electrodes should be placed on opposite sides along and perpendicular to the axis of this dipole. The location of the EASSR source in the brain varies with varying modulation frequencies. EASSRs to modulation frequencies in the 40 Hz range (20–60 Hz) originate from sub-cortical sources [7]. Whether it is possible to adequately record EASSRs with a specific combination of analysis and reference electrodes thus depends on the selected modulation frequency. EASSRs were also recorded at suprathreshold stimulation levels for the same subjects, and for the modulation frequencies we tested in the 40 Hz range, it was still possible to record reliable EASSRs when reference electrode Fp_z was selected (data not presented). Reference electrode Fp_z is also often used in clinical ABR and ASSR measurements in infants [44]. It should be noted that referencing the data to Fp_z can lead to increased noise levels, resulting in reduced EASSR detections or requiring longer measurement times.

Only one subject had symmetric CI artifacts, that did not scale with increasing stimulation amplitude. CI artifacts had a contribution at the modulation frequency for all other subjects.

The amplitude A_m at the modulation frequency, consisting of contributions from the STIM artifact and the neural response, reduces with increasing interpolation duration. The A_m difference for subsequent interpolation durations was compared to the noise level after averaging. The STIM artifact duration is the interpolation duration for which this difference becomes smaller than the noise level. Because we look at the saturation of A_m, and not at its absolute level, this method can also be applied to recordings with stimulation at suprathreshold levels. Furthermore, the time T over which the EEG signals were averaged plays an important role here, since the noise level is dependent on this. The noise level is reduced with a factor $\sqrt{2}$ each time the averaging time is doubled. The STIM artifact duration thus determines whether the STIM artifact can be removed by linear interpolation for recording time T. For longer recording times, the contribution of the STIM artifact may not be below the noise level and the STIM artifact is possibly not completely removed by applying linear interpolation.

For stimulation at 500 pps, the STIM artifact can be removed at contralateral recording electrodes with a linear interpolation. In the contralateral hemisphere, the variability of θ (for stimulation at 500 pps) and D was smaller for more frontal reference electrodes, see Figs. 9 and 11. Therefore, for recording electrodes in the contralateral hemisphere, the chance that the STIM artifact duration is longer than the maximum possible interpolation duration is reduced by choosing a more frontal reference electrode.

Linear interpolation is not sufficient to examine responses at ipsilateral recording electrodes or for stimulation pulse rates higher than 500 pps. Other stimulation artifact removal methods should therefore be examined. Further modeling of CI artifacts could allow template subtraction or adaptive filter design for CI artifact removal. Multichannel methods could possibly be used, with the disadvantage – for CI fitting purposes – that these require a more expensive setup and more subject preparation time.

Only subjects with Cochlear Nucleus® implants participated in this study. However, the stimulation artifacts caused by implants from other manufacturers should be examined, using the methods presented here. Differences can be expected, as other manufacturers use different clinical parameters.

In this study, a 64-channel recording set-up was used, which allowed to investigate the influence of reference electrode position on the CI artifact characteristics. Setups with less channels can usually be operated at higher sample rates and have low pass filters with higher cut-off frequencies, which could result in shorter STIM artifact durations. The method presented in this study can still be used to determine the STIM artifact duration and the required interpolation duration.

In this study, subjects were only tested at subthreshold stimulation amplitudes. STIM artifact durations may be larger for suprathreshold stimulation amplitudes. Larger stimulation amplitudes may result in larger CI artifact amplitudes. Assuming that the decay constant does not change, it takes longer for larger CI artifact amplitudes to decay below the noise level. However, 11 subjects were tested, where the stimulation amplitudes used were just below the subject's behavioral T levels. The range of T levels observed in these subjects is quite diverse, resulting in maximum stimulation pulse amplitudes used between 108 and 190 cu, and between 86 and 167 cu for stimulation at 500 and 900 pps, respectively. We would argue that the results from this study are representative, since a wide variety of stimulation levels was used.

Here only one stimulation electrode in the middle of the array was used. The stimulation electrode is not expected to have much influence on the CI artifact characteristics. Future research should focus on the influence of stimulation electrode position on CI artifact characteristics, which can be evaluated with the tools presented in this study.

5. Conclusion

In most subjects, the CI artifact was at least partly caused by the STIM artifact. Based on the data presented in Figs. 5 and 9–11, it is not recommended to use average reference for EASSR measurements. CI artifact AGF slopes and intercepts and STIM artifact durations are larger in the contralateral hemisphere for the average reference configuration than C_z or Fp_z reference. In the contralateral hemisphere, the reference electrode has a significant influence on the CI artifact AGF slope and intercept for stimulation at 500 pps and on the STIM artifact duration. In the contralateral hemisphere, smaller variabilities in CI artifact AGF slopes (at 500 pps) and STIM artifact durations were observed when more frontal reference electrodes were used. STIM artifact durations were between 0.7 and 1.7 ms and 0.7 and 2 ms, at contralateral and ipsilateral recording electrodes, respectively. This should make it possible to remove the CI artifact at the contralateral recording electrodes with a linear interpolation in most subjects, for stimulation at 500 pps. For stimulation at 900 pps or for stimulation at 500 pps at ipsilateral recording electrodes, more advanced CI artifact attenuation methods are needed.

Acknowledgments

The authors would like to thank all subjects who participated in the study. Furthermore, a special thanks goes out to Robert Luke and Tom Francart for their valuable feedback throughout the study. This research work was carried out in the frame of Research Project FWO nr. G.066213 'Objective mapping of cochlear implants', IWT Project (IWT, 110722) 'Signal processing and automatic fitting for next generation cochlear implants' and KU Leuven Research Council CoE PFV/10/002 (OPTEC). The second author is supported with a Ph.D. grant by the Hermesfonds (141243). None of the authors have potential conflicts of interest to be disclosed.

References

[1] J.C. Lilly, J.R. Hughes, E.C. Alvord, T.W. Galkin, Brief, noninjurious electric waveform for stimulation of the brain, Science 121 (1955) 468–469.
[2] T. Boons, J.P.L. Brokx, I. Dhooge, J.H.M. Frijns, L. Peeraer, A. Vermeulen, J. Wouters, A. van Wieringen, Predictors of spoken language development following pediatric cochlear implantation, Ear Hear. 33 (5) (2012) 617–639.
[3] C.J. Brown, M.L. Hughes, B. Luk, P.J. Abbas, A. Wolaver, J. Gervais, The relationship between EAP and EABR thresholds and levels used to program the nucleus 24 speech processor: data from adults, Ear Hear. 21 (2) (2000) 151–163.
[4] D. Cafarelli Dees, N. Dillier, W.K. Lai, E. von Wallenberg, B. van Dijk, F. Akdas, M. Aksit, C. Batman, A. Beynon, S. Burdo, J.-M. Chanal, et al., Normative findings of electrically evoked compound action potential measurements using the neural response telemetry of the Nucleus CI24M cochlear implant system, Audiol. Neurotol. 10 (2) (2005) 105–116.
[5] M.L. Hughes, C.J. Brown, P.J. Abbas, A.A. Wolaver, J.P. Gervais, Comparison of EAP thresholds with MAP levels in the Nucleus 24 cochlear implant: data from children, Ear Hear. 21 (2) (2000) 164–174.
[6] C.A. Miller, N. Hu, F. Zhang, B.K. Robinson, P.J. Abbas, Changes across time in the temporal responses of auditory nerve fibers stimulated by electric pulse trains, J. Assoc. Res. Otolaryngol. 9 (1) (2008) 122–137.
[7] A.T. Herdman, O. Lins, P. Van Roon, D.R. Stapells, M. Scherg, T.W. Picton, Intracerebral sources of human auditory steady-state responses, Brain Topogr. 15 (2) (2002) 69–86.
[8] T.W. Picton, M.S. John, A. Dimitrijevic, D. Purcell, Human auditory steady-state responses, Int. J. Audiol. 42 (4) (2003) 177–219.
[9] R.A. Dobie, M.J. Wilson, A comparison of *t* test, *F* test, and coherence methods of detecting steady-state auditory-evoked potentials, distortion-product otoacoustic emissions, or other sinusoids, J. Acoust. Soc. Am. 100 (4) (1996) 54–71.
[10] M. Hofmann, J. Wouters, Electrically evoked auditory steady state responses in cochlear implant users, J. Assoc. Res. Otolaryngol. 11 (2) (2010) 267–282.
[11] X. Li, K. Nie, F. Karp, K.L. Tremblay, J.T. Rubinstein, Characteristics of stimulus artifacts in EEG recordings induced by electrical stimulation of cochlear implants, in: 3rd International Conference on Biomedical Engineering and Informatics, 2010, pp. 799–803.
[12] M. Hofmann, J. Wouters, Improved electrically evoked auditory steady-state response thresholds in humans, J. Assoc. Res. Otolaryngol. 13 (4) (2012) 573–589.
[13] R.J. Ilmoniemi, J.C. Hernandez-pavon, N.N. Mäkelä, J. Metsomaa, T.P. Mutanen, J. Sarvas, Dealing with artifacts in TMS-evoked EEG, in: Annual International Conference of the IEEE Engineering in Medicine and Biology Society, 2015, pp. 230–233.
[14] P.M. Gilley, A. Sharma, M. Dorman, C.C. Finley, A.S. Panch, K. Martin, Minimization of cochlear implant stimulus artifact in cortical auditory evoked potentials, Clin. Neurophysiol. 117 (8) (2006) 1772–1782.
[15] F.-C. Jeng, P.J. Abbas, C.J. Brown, C.A. Miller, K.V. Nourski, B.K. Robinson, Electrically evoked auditory steady-state responses in Guinea pigs, Audiol. Neurootol. 12 (2) (2007) 101–112.
[16] B.A. Martin, Can the acoustic change complex be recorded in an individual with a cochlear implant? Separating neural responses from cochlear implant artifact, J. Am. Acad. Audiol. 18 (2) (2007) 126–140.
[17] D.P. Allen, E.L. Stegemöller, C. Zadikoff, J.M. Rosenow, C.D. MacKinnon, Suppression of deep brain stimulation artifacts from the electroencephalogram by frequency-domain Hampel filtering, Clin. Neurophysiol. 121 (8) (2010) 1227–1232.
[18] A. Santillán-Guzmán, U. Heute, M. Muthuraman, U. Stephani, A. Galka, DBS artifact suppression using a time–frequency domain filter, in: Annual International Conference of the IEEE Engineering in Medicine and Biology Society, 2013, pp. 4815–4818.
[19] D. Sinkiewicz, L. Friesen, B. Ghoraani, Analysis of cochlear implant artifact removal techniques using the continuous wavelet transform, in: Annual International Conference of the IEEE Engineering in Medicine and Biology Society, 2014, pp. 5482–5485.
[20] M. Yochum, S. Binczak, A wavelet based method for electrical stimulation artifacts removal in electromyogram, Biomed. Signal Process. Control 22 (2015) 1–10.
[21] B.H. Boudreau, K. Englehart, A.D.C. Chan, P. Parker, Subthreshold training: a novel approach to stimulus artifact cancellation in somatosensory evoked potential recordings, in: 25th Annual International Conference of the IEEE EMBS, 2003, pp. 2659–2662.
[22] B.H. Boudreau, K.B. Englehart, a.D.C. Chan, P.a. Parker, Reduction of stimulus artifact in somatosensory evoked potentials: segmented versus subthreshold training, IEEE Trans. Biomed. Eng. 51 (7) (2004) 1187–1195.
[23] P. Grieve, P. Parker, B. Hudgins, K. Englehart, Nonlinear adaptive filtering of stimulus artifact, IEEE Trans. Biomed. Eng. 47 (3) (2000) 389–395.
[24] S. Kohli, A.J. Casson, Removal of transcranial AC current stimulation artifact from simultaneous EEG recordings by superposition of moving averages, in: Annual International Conference of the IEEE Engineering in Medicine and Biology Society, 2015, pp. 3436–3439.
[25] M. Mancini, M.C. Pellicciari, D. Brignani, P. Mauri, C. De Marchis, C. Miniussi, S. Conforto, Automatic artifact suppression in simultaneous tDCS-EEG using adaptive filtering, in: Annual International Conference of the IEEE Engineering in Medicine and Biology Society, 2015, pp. 2729–2732.
[26] V. Parsa, P. Parker, R. Scott, N. Brunswick, Convergence characteristics of two algorithms in non-linear stimulus artefact cancellation for electrically evoked potential enhancement, Med. Biol. Eng. Comput. 36 (2) (1998) 202–214.
[27] L.M. Friesen, T.W. Picton, A method for removing cochlear implant artifact, Hear. Res. 259 (2010) 95–106.
[28] M. McLaughlin, A.L. Valdes, R.B. Reilly, F.-G. Zeng, Cochlear implant artifact attenuation in late auditory evoked potentials. A single channel approach, Hear. Res. 302 (2013) 84–95.
[29] D.A. Wagenaar, Real-time multi-channel stimulus artifact suppression by local curve fitting, J. Neurosci. Methods 120 (2) (2002) 113–120.
[30] T. Wichmann, A digital averaging method for removal of stimulus artifacts in neurophysiologic experiments, J. Neurosci. Methods 98 (1) (2000) 57–62.

[31] L.F. Heffer, J.B. Fallon, A novel stimulus artifact removal technique for high-rate electrical stimulation, J. Neurosci. Methods 170 (2) (2008) 277–284.
[32] U. Hoffmann, W. Cho, A. Ramos Murguialday, T. Keller, Detection and removal of stimulation artifacts in electroencephalogram recordings, in: Annual International Conference of the IEEE Engineering in Medicine and Biology Society, EMBS, 2011, pp. 7159–7162.
[33] D.D.E. Wong, K.A. Gordon, Beamformer suppression of cochlear implant artifacts in an electroencephalography dataset, IEEE Trans. Biomed. Eng. 56 (12) (2009) 2851–2857.
[34] I. Akhoun, C.M. McKay, W. El-deredy, Electrically evoked compound action potential artifact rejection by independent component analysis: technique validation, Hear. Res. 302 (2013) 60–73.
[35] J.C. Hernandez-Pavon, J. Metsomaa, T. Mutanen, M. Stenroos, H. Mäki, R.J. Ilmoniemi, J. Sarvas, Uncovering neural independent components from highly artifactual TMS-evoked EEG data, J. Neurosci. Methods 209 (1) (2012) 144–157.
[36] R.J. Korhonen, J.C. Hernandez-Pavon, J. Metsomaa, H. Mäki, R.J. Ilmoniemi, J. Sarvas, Removal of large muscle artifacts from transcranial magnetic stimulation-evoked EEG by independent component analysis, Med. Biol. Eng. Comput. 49 (4) (2011) 397–407.
[37] J. Metsomaa, J. Sarvas, R.J. Ilmoniemi, Multi-trial evoked EEG and independent component analysis, J. Neurosci. Methods 228 (2) (2014) 15–26.
[38] N.C. Rogasch, R.H. Thomson, F. Farzan, B.M. Fitzgibbon, N.W. Bailey, J.C. Hernandez-Pavon, Z.J. Daskalakis, P.B. Fitzgerald, Removing artefacts from TMS-EEG recordings using independent component analysis: importance for assessing prefrontal and motor cortex network properties, NeuroImage 101 (2014) 425–439.
[39] R. Ruach, R. Mitelman, E. Sherman, O. Cohen, Y. Prut, An assumption-free quantification of neural responses to electrical stimulations, J. Neurosci. Methods 254 (2015) 10–17.
[40] F.C. Viola, M. De Vos, J. Hine, P. Sandmann, S. Bleeck, J. Eyles, S. Debener, Semi-automatic attenuation of cochlear implant artifacts for the evaluation of late auditory evoked potentials, Hear. Res. 284 (2012) 6–15.
[41] F.C. Viola, J.D. Thorne, S. Bleeck, J. Eyles, S. Debener, Uncovering auditory evoked potentials from cochlear implant users with independent component analysis, Psychophysiology 48 (11) (2011) 1470–1480.
[42] J. Wolfe, E. Schafer, Programming Cochlear Implants, Tech. Rep., 2010.
[43] H.H. Jasper, The 10–20 electrode system of the International Federation, Electroencephalogr. Clin. Neurophysiol. 10 (2) (1958) 371–375.
[44] J.W. Hall, New Handbook of Auditory Evoked Responses, 2007.